Neurosci. Bull. April, 2022, 38(4):386–402
https://doi.org/10.1007/s12264-022-00841-w

www.neurosci.cn
www.springer.com/12264

ORIGINAL ARTICLE

Referred Somatic Hyperalgesia Mediates Cardiac Regulation by the Activation of Sympathetic Nerves in a Rat Model of Myocardial Ischemia

Xiang Cui[1] · Guang Sun[1,2] · Honglei Cao[3] · Qun Liu[4] · Kun Liu[1] · Shuya Wang[1] · Bing Zhu[1] · Xinyan Gao[1]

Received: 24 August 2021 / Accepted: 13 December 2021 / Published online: 26 April 2022

Abstract Myocardial ischemia (MI) causes somatic referred pain and sympathetic hyperactivity, and the role of sensory inputs from referred areas in cardiac function and sympathetic hyperactivity remain unclear. Here, in a rat model, we showed that MI not only led to referred mechanical hypersensitivity on the forelimbs and upper back, but also elicited sympathetic sprouting in the skin of the referred area and C8–T6 dorsal root ganglia, and increased cardiac sympathetic tone, indicating sympathetic-sensory coupling. Moreover, intensifying referred hyperalgesic inputs with noxious mechanical, thermal, and electro-stimulation (ES) of the forearm augmented sympathetic hyperactivity and regulated cardiac function, whereas deafferentation of the left brachial plexus diminished sympathoexcitation. Intradermal injection of the α_2 adrenoceptor (α_2AR) antagonist yohimbine and agonist dexmedetomidine in the forearm attenuated the cardiac adjustment by ES. Overall, these findings suggest that sensory inputs from the referred pain area contribute to cardiac functional adjustment *via* peripheral α_2AR-mediated sympathetic-sensory coupling.

Keywords Sympathetic-sensory coupling · Neuromodulation · Referred pain · α_2 adrenoceptor · Cardioprotection

Introduction

Referred pain in the chest and the left upper arm as a consequence of myocardial ischemia (MI), has been studied extensively [1, 2]. Cardiac referred pain is a result of the convergence and facilitation of cardiac and somatic inputs in the thoracic spinal cord and the integrated projections to various brain regions [1, 3–7]. Spinothalamic tract neurons alone, or together with spinoreticular tract neurons in the upper thoracic spinal cord [3], lead to sensations of angina and pain referred to overlying somatic structures [5]. Cell bodies of the heart and coronary arterial afferents are located in the dorsal root ganglia (DRGs) of T1–T5 and may slightly extend into the upper or lower segments [8]. The cardiac afferent fiber-endings are distributed more densely in the anterior region of the left ventricle than in other parts of the heart [9], and they may transmit more noxious sensation to the spinal cord and supraspinal structures after injury to the myocardium. Although pain is an unpleasant feeling, it plays a positive role in the regulation of homeostasis [10] and is pivotal in avoiding tissue damage and risks. Recent studies have revealed that peripheral nociceptive stimulation induces cardioprotection in an MI model, as the activation of somatic high-threshold C-fibers leads to the release of

Supplementary Information The online version contains supplementary material available at https://doi.org/10.1007/s12264-022-00841-w.

✉ Bing Zhu
zhubing@mail.cintcm.ac.cn

✉ Xinyan Gao
xinyangao2001@msn.com

1 Department of Physiology, Institute of Acupuncture and Moxibustion, China Academy of Chinese Medical Sciences, Beijing 100700, China

2 Research Center of Traditional Chinese Medicine, The Affiliated Hospital of Changchun University of Chinese Medicine, Changchun, Jilin 130021, China

3 Department of Cardiology, Jining No. 1 People's Hospital, Jining 272100, Shandong, China

4 Department of Needling Manipulation, Institute of Acupuncture and Moxibustion, China Academy of Chinese Medical Sciences, Beijing 100700, China

norepinephrine (NE) and bradykinin from the cardiac sympathetic nerve *via* a dorsal root reflex [11, 12]. For instance, topical capsaicin-mediated stimulation directly activates the cutaneous C-fibers and has a cardioprotective effect, which supports its clinical application [11]. We hypothesized that sensitized afferents from the cardiac referred pain cutaneous area initiate sustained somatic irritation by sympathetic sprouting and boost the regulation of functional cardiac homeostasis and preservation of the myocardium.

Sympathetic hyperexcitation is a vital manifestation of MI [13]. The cardiac innervation consists of the sympathetic and parasympathetic (vagus) nervous systems. Sympathetic innervation originates from the stellate ganglia and superior cervical ganglion, while the anterior myocardium of the left ventricle is predominantly controlled by the superior cervical ganglion [14]. MI with decreased left ventricular systolic function results in abrupt sympathetic hyperactivation and elevated release of NE in the postganglionic sympathetic fiber terminals, which acts as cardiac functional compensation to preserve the circulation volume through the enhancement of vascular and ventricular resistance [15, 16]. However, hyperactive sympathetic activity is prone to induce ventricular arrhythmias or even cardiac death and acts as a double-edged sword [17, 18]. Previous studies have demonstrated that sympathetic hyperactivity leads to fiber terminal sprouting into the myocardium and surrounding the infarcted area, which may strengthen the heart contractility in response to coronary ischemia [18]. A recent study demonstrated that the cardiac TRPV1 receptor contributes to sympathetic hyperactivity and ventricular arrhythmogenesis, while specific depletion of cardiac TRPV1-positive fibers using resiniferatoxin potentially attenuates the arrhythmogenic ventricular sympathoexcitation [19]. This evidence suggested that local interactions between cardiac afferents and sympathetic outputs regulate the homeostasis of cardiac functions.

Sympathetic-sensory coupling has been commonly reported in skin and DRGs under conditions of chronic pain, neuropathic pain, inflammatory pain, or complex regional pain syndrome, contributing to the exacerbation and sustenance of the peripheral and central sensitization for hyperalgesia [20–23]. Sprouted sympathetic terminals can release NE that binds to the α_2 adrenoceptors (α_2AR) in peripheral structures and mediates the sympathetic-sensory interaction and sensitization [23–25]. Sympathectomy or pharmacological sympathetic blockade by α_2ARs antagonists suppresses the sprouting of the sympathetic terminals and ameliorates pain [25, 26]. However, it is yet to be fully understood if this sympathetic-sensory coupling occurs in MI along with structural abnormality and whether it has protective functional significance.

To address these questions, we first investigated whether sympathetic sprouting and sensory coupling structures appear in the referred somatic area and thoracic DRGs under MI pathology. We also applied behavioral tests to assess somatic hypersensitivity on referred areas such as the forearm and upper back in MI rats. Moreover, *in vivo* electrophysiological recording and echocardiography were applied to evaluate the changes in sympathetic tone and cardiac function in MI rats. Under this paradigm, we accentuated inputs from the referred hyperalgesic areas with nociceptive stimulation on the forelimb or attenuated inputs by deafferentation to assess the changes in cardiac activity and autonomic nerve functions. Finally, we used pharmacological strategies to demonstrate the participation of α_2AR-mediated sensory-sympathetic coupling in cardiac referred hypersensitivity and the subsequent positive regulation of cardiac function after MI.

Materials and Method

Animals

Adult male Sprague–Dawley rats (220–250 g) were obtained from the Laboratory Animal Center of China Academy of Military Medical Sciences [license number: SCXK–(Military)–2012–0004] and used for all experiments. The rats were housed in a climate-controlled environment (25 ± 2°C and 50% ± 15% humidity) with *ad libitum* access to food and water under an alternating 12-h cycle of dark and light; they were maintained in line with the recommendations in the Guide for the Care and Use of Laboratory Animals of the National Institutes of Health. This protocol was approved by the Committee on Ethics of Animal Experiments of the Institute of Acupuncture and Moxibustion, China Academy of Chinese Medical Sciences. All rats were acclimatized for at least 1 week upon arrival before any procedure was administered.

Myocardial Ischemia Model

The MI model was created as previously described [27]. Briefly, rats were anesthetized by intraperitoneal injection of 50 mg/kg sodium pentobarbital (Sigma-Aldrich, St. Louis, MO, USA) and then intubated and ventilated (CWE, SAR-830, USA) during the surgical procedure. The pericardium was exposed and removed *via* a horizontal incision through the muscle between the left fourth and fifth intercostal spaces. The left anterior descending coronary artery (LAD) was permanently ligated with a 6–0 silk suture and the ligation area was width: 1–2 mm, depth: 0.5–1 mm. Rats in the control group were subjected to the same procedure without ligation of the LAD.

Determination of Cardiac Tissue Injury in MI

TTC staining was applied to confirm the MI as previously described [28]. At 7 days after LAD ligation, each rat was anesthetized and sacrificed, and then the heart was quickly excised and washed in saline before being frozen at –20°C. After freezing for 30 min, the heart was cut into 6–7 slices and incubated with 1% 2,3,5-triphenyl tetrazolium chloride (TTC, Sigma-Aldrich, St. Louis, USA) diluted in PBS (pH 7.4) for 20 min at 37°C in darkness. Infarcted myocardium appeared paler after TTC staining than the surrounding myocardium (Fig. S1C).

Skin Plasma Protein Extravasation in MI Rats

At 7 days after MI operation, rats were anesthetized with 4% isoflurane and then placed on a feedback heating pad (H–KWDY–III, Nanjing Xin Xiao Yuan Biotech, China). Evans blue (EB) solution (50 mg/kg; 50 mg/mL in saline, Sigma-Aldrich) was injected into the lateral caudal vein. Thirty minutes to 1 h after EB injection, the numbers of blue plasma extravasation points were counted and recorded on a rat somite chart. The hair of the forelimb, chest, and upper back was shaved using a commercially available hair removal cream (VEET, China). Great care was given to avoid extra irritation of the skin when shaving and handling during the EB test.

Somatic Referred Hypersensitivity in MI Rats

To determine whether referred somatic hypersensitivity occurred in MI model rats, we tested the mechanical sensitivity on the forelimb and upper back as previously described [29], where plasma extravasation and EB staining had been found on day 7. The hair was removed using a shaver (KP-3000, Codos, China) one day before measurement. An electronic von Frey anesthesiometer (IITC 2390; Life Science, USA) supplied with a rigid tip (0.8 mm diameter) was applied to the forelimb and upper back before MI modeling and 3, 7, and 28 days after MI surgery. Rats were acclimatized in a transparent partitioned chamber with some holes around its sides for 30 min. The tip of the anesthesiometer was perpendicularly applied to the testing areas five times for 3 s each at 10-s intervals. A rapid vertical or horizontal movement of the forelimb and quick recoil of the upper back were considered to be positive responses.

Immunofluorescence Staining

Three and 7 days after the MI operation, rats were anesthetized with sodium pentobarbital (50 mg/kg, i.p.) and subjected to intracardiac perfusion with 0.9% saline followed by 4% paraformaldehyde. DRGs at the C8–T6 spinal segments and the referred hypersensitive skin (3 × 3 mm^2) at PC 6, located 3 mm lateral and distal to the wrist joint and between the radius and ulna in the referred forelimb [30], were dissected out and then postfixed in 4% paraformaldehyde and dehydrated in 25% sucrose for 48 h for cryoprotection. Sections were cut at 40 μm and 20 μm for DRGs and skin, respectively, on a cryostat (CM1950, Leica). The sections were blocked in 3% normal donkey serum and 0.5% Triton X-100 in phosphate buffer (PB) for 1 h at room temperature. After blocking, the DRG and skin sections were incubated overnight with the fluorescent dye NeuroTrace 530/615 (Nissl) (1:2000, N21482, Invitrogen) to label sensory neurons in the DRGs, tyrosine hydroxylase (TH) (ab112,1:500, Abcam, Cambridge, UK) to visualize sympathetic fibers in the DRGs and skin, and calcitonin gene-related peptide (CGRP) (ab81887, 1:1000, Abcam) to visualize nociceptive sensory neurons in the DRGs and peripheral sensory fibers in the skin. After overnight incubation with primary antibodies at 4°C, the slides were washed three times in PB and incubated with appropriate AlexaFluor-conjugated secondary antibodies (1:500; Molecular Probes, Eugene, OR, USA) for 1 h at room temperature, then coverslipped with 50% glycerin and photographed on a confocal imaging system (FV1200, Olympus, Tokyo, Japan). Adobe Photoshop CC was used to improve the quality of images. The numbers of CGRP-immunoreactive(IR) neurons and the lengths of TH-IR and CGRP-IR fibers were calculated using microimaging software (cellSens standard 1.11, Olympus).

Western Blot Analysis

The DRGs of the left C8–T6 spinal segments and the referred hypersensitive skin (3 × 3 mm^2) on the left forelimb were removed and ground in liquid nitrogen, then the samples were lysed with RIPA buffer (Sigma) containing a protease inhibitor. Protein concentration was evaluated with a BCA protein quantitative analysis kit. Protein samples were resolved on 10% SDS-PAGE gel and transferred onto a polyvinylidene fluoride membrane (Millipore, Bedford, MA, USA). After being blocked with 3% BSA-TBST, the membranes were incubated with primary antibodies against TH (1:8000; ab112, Abcam), CGRP (1:500; ab47027, Abcam), and GAPDH (1:20000; YM3029, Immunoway) overnight at 4°C. Subsequently, the membranes were incubated with appropriate HRP-conjugated secondary antibodies (anti-rabbit IgG, anti-mouse IgG, 1:10000; Molecular Probes, Eugene, OR, USA) for 1 h. Protein expression was visualized using ChemiDoc Touch V3 Western Blot Workflow (Bio-Rad, USA) and quantified by ImageJ (National Institutes of

Health). The intensity of each protein was normalized to that of GAPDH and then used for analysis.

Electrocardiogram Recording

Standard limb lead II surface ECG was recorded *via* an Animal Bio Amp (ADInstruments, NSW, Australia) and LabChart professional software (version 8.0) containing an ECG module during the MI model operation (gain, 1000 Hz; low-cut filter, 200 Hz; high-cut filter, 0.3 Hz). Elevation of the ST segment beyond 0.1 mV represents successful LAD ligation. The mean ECG voltage 13 ms after the peak of the S wave was defined as the value of the ST segment, as described previously [31].

Cardiac Sympathetic and Vagus Nerve Activity Recording

To assess cardiac autonomic nerve activity and function in MI rats, cardiac sympathetic nerve branches from the superior cervical ganglion (SCG) and cervical vagal nerve were dissociated and recorded using a platinum wire electrode (50 μm). The SCG is spindle-shaped, located at the bifurcations of the common carotid arteries. The carotid branch, which leaves the cranial pole of the ganglion and follows the internal carotid artery, was used for recording [32]. The cervical vagal nerve was exposed and ligated at the middle; the proximal portion was recorded with a pair of platinum hook electrodes (Fig. 4). The signal was amplified by a pre-amplifier (AM-1800; A–M Systems, Sequim, WA, USA) and collected through the Powerlab data acquisition system using LabChart 8.0 software (ADInstruments, NSW, Australia). Spike frequency was analyzed using spike histograms of LabChart 8.0 (gain, 1000 Hz; low-cut filter, 100 Hz; high-cut filter, 1000 Hz).

Echocardiography

Rats were anesthetized with 4% isoflurane at 7 days after LAD ligation. Echocardiography was applied to evaluate cardiac function using the Vevo 2100 Imaging System (Visual Sonics, ON, Canada) equipped with a 40-MHz probe as previously described [33]. M-mode tracings in the parasternal short-axis view were used to measure the left ventricular internal diameter at end-diastole and end-systole; the left ventricular ejection fraction (EF), heart rate (HR), and cardiac output (CO) were also calculated.

Somatic Stimulation of the Referred Area of MI Rats

Somatic stimulation of the referred area of the MI model was applied to augment the somatic referred hypersensitivity. Cardiac sympathetic nerve activity (SNA), vagal nerve activity (VNA), and HR were recorded when brush (6 g), pinch, electrical stimulation (3 mA, 15 Hz), and thermal stimuli (48°C) were randomly applied to the left forelimb for 30 s each at 5-min intervals; corresponding areas on the lower limbs were given the same stimuli for controls. For forelimb stimulation, the area 3 mm lateral and distal to the wrist joint and between the radius and ulna was selected (the PC6 acupoint in traditional Chinese medicine and acupuncture; see Fig. 1). This point was also found to be EB-positive in the extravasation test. Considering that somatic noxious stimulation to various spinal segments is capable of altering cardiac function and SNA through the somato-sympathetic reflex in healthy controls [34, 35], and that the aim of the present study was to explore the potential role of the referred hypersensitized area in cardiac functional self-regulation under MI, the ipsilateral hindlimb SP6 acupoint was selected as a control for PC6. SP6 is near the ankle joint, at the level of the superior border of the medial malleolus between the posterior border of the tibia and the anterior border of the Achilles tendon [36]. After electrophysiological recording in intact animals, the left brachial plexus deep to the neck muscles [37], was severed to assess the influence of referred somatic hypersensitivity on autonomic and cardiac activity.

Drug Administration

To verify the role of α_2ARs in sympathetic-sensory coupling in the referred skin areas, rats were randomized to receive the α_2AR agonist dexmedetomidine (DEX, 5 μg/20 μL) (HY-B0409A, Medchemexpress), and the α_2AR antagonist yohimbine hydrochloride (YOB, 5 μg/20 μL) (HY–N0127, Medchemexpress) [24]. These drugs were dissolved in distilled water and intradermally injected at PC6 with a 20 μL microsyringe. Twenty microliters of saline were intradermally injected as control.

Statistical Analysis

The Shapiro-Wilk test was used to test for normal distribution in all data; only data that passed the normality test are presented in graphs as the mean ± SEM. The methods for statistical analyses for each study are noted in the figure legends. All analyses were performed using GraphPad Prism 8 (GraphPad Software, Inc., San Diego, CA, USA), and only $P < 0.05$ was considered statistically significant.

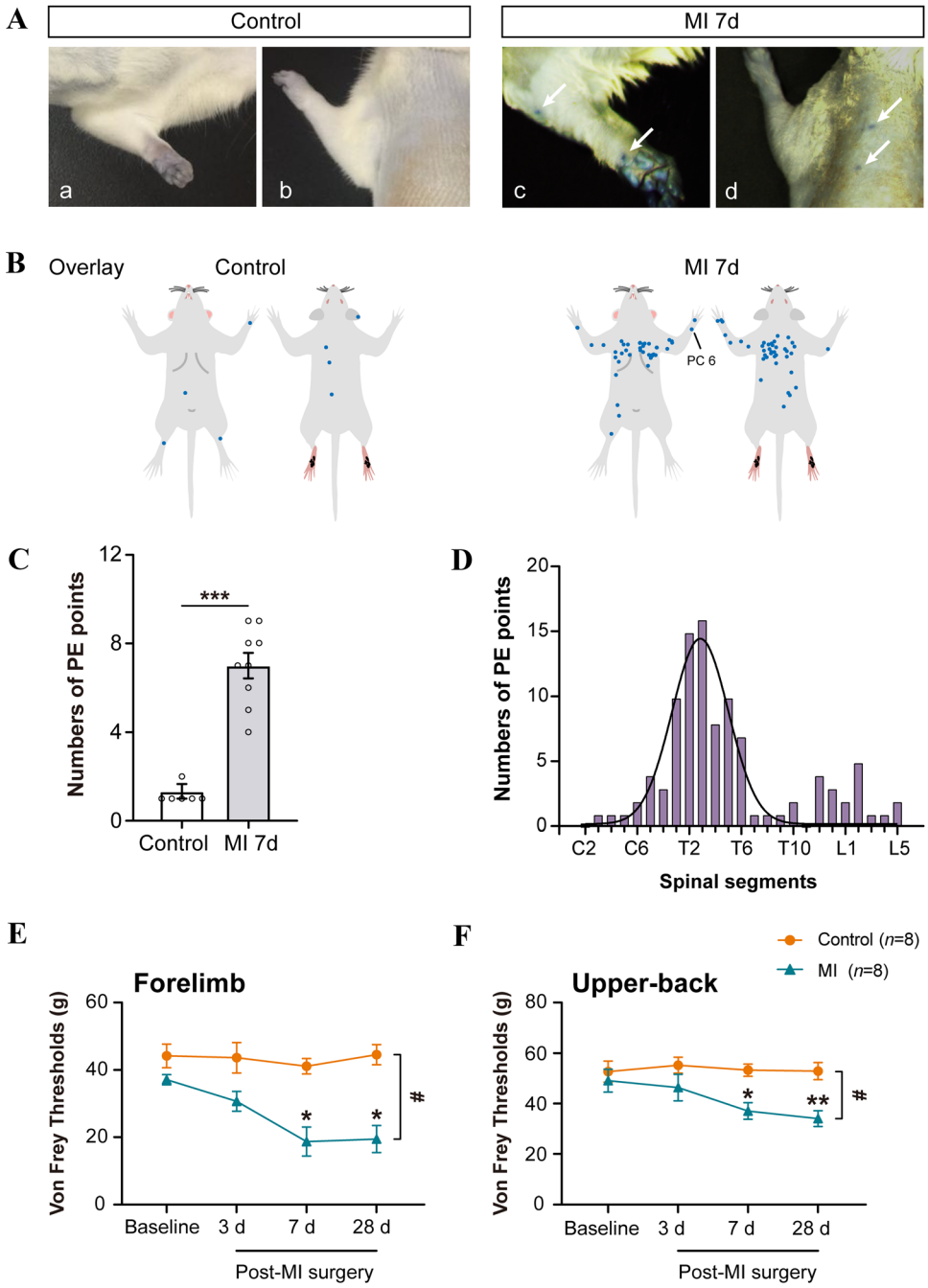

Fig. 1 MI induces plasma extravasation and referred mechanical hypersensitivity in skin. **A** Representative images showing EB plasma extravasation (PE) points in the left forelimb (**Ac**) and upper-back (**Ad**) after MI, as compared to the control (**Aa**, **b**). **B** Schematics of merged PE points in the skin from control (n = 6) and MI rats (n = 9, 7 days post-MI). **C** Quantification of PE points in both groups (***P <0.001, independent t-test). **D** PE points are mainly distributed in dermatomes of the T1–T5 spinal segments. **E**, **F** Withdrawal threshold to mechanical stimulation (von Frey filaments) in the forelimb and upper-back is lower in MI rats than in controls (n = 8/group. *P <0.05, **P <0.01; $^{\#}P$ <0.05, two-way ANOVA with Bonferroni test).

Results

Neurogenic Inflammation and Referred Somatic Mechanical Hypersensitivity After MI

To test the distribution of the area of referred hypersensitivity induced by MI, EB was injected into the lateral caudal vein at 7 days after MI operation. EB binds to plasma proteins and is exuded from the enlarged capillary space caused by the neurogenic inflammatory reaction [38]; as a result of which, blue spots were observed from 0.5 to 1 h after injection (Fig. 1A, Fig. S2). The results indicated that the areas of EB extravasation were mainly on the left chest, forelimb, and upper-back regions from C6 to T6 (Fig. 1B, D), covering spinal segments receiving afferents from skin areas the same as and adjacent to the heart [39], while EB staining rarely appeared in healthy control rats (Fig. 1B, C).

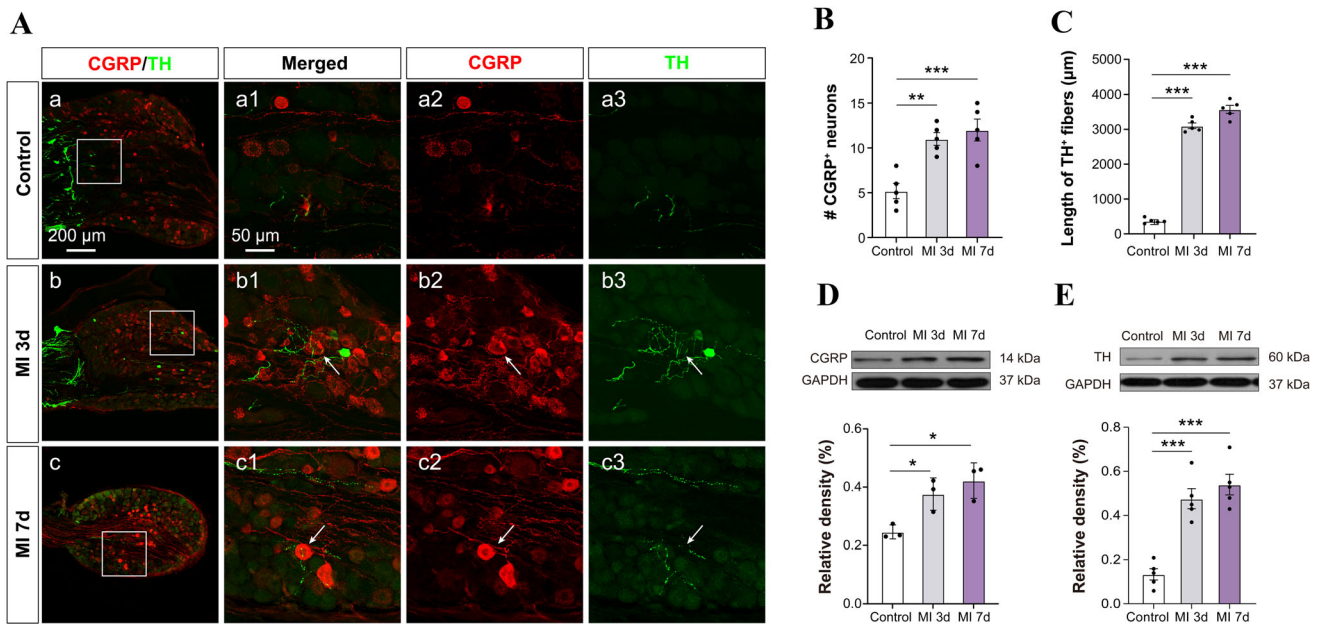

Fig. 2 Sprouting of sympathetic post-ganglionic fibers in DRGs after MI. **A** Representative images of immunoreactivity to calcitonin gene-related peptide (CGRP, red, a marker for peptidergic nociceptive neurons) and tyrosine hydroxylase (TH, green) which labels adrenergic fibers in the DRGs of control and MI rats at 3 and 7 days after LAD ligation. **a**1–3: the higher power views of the boxed area in **a** (the same for **b** and **c**). White arrows indicate sprouted sympathetic terminals. **B, C** Quantification of the number of CGRP+ neurons and the length of TH+ fibers in the DRGs (n = 4/group, $^{**}P$ <0.01, $^{***}P$ <0.001). **D, E** Western blots showing increased levels of CGRP and TH protein expression in the C8–T6 DRGs in rats at days 3 and 7 post-MI (n = 3–4/group, $^{*}P$ <0.05, $^{***}P$ <0.001). One-way ANOVA with least significant difference multiple comparisons in **B–E**.

Next, we determined whether the EB-permeable skin area was mechanically hypersensitive using electronic Von Frey measurement. The data indicated that the mechanical thresholds for the forelimb and upper-back in MI rats were significantly lower on days 7 and 28 after MI than those at baseline or in the control group, suggesting that MI modeling induced referred somatic hyperalgesia in the forelimb and upper-back (Fig. 1E, F). These results collectively demonstrated that MI caused somatic neurogenic inflammation and mechanical hypersensitivity in the forelimb and upper-back at spinal segments the same as and adjacent to the heart.

MI Induces Sympathetic Post-ganglionic Fiber Sprouting in DRGs and Skin

Increasing numbers of studies have reported the sprouting of sympathetic post-ganglionic fibers to form a sympathetic-sensory coupling structure in DRGs and skin under neuropathic and inflammatory pain conditions that play a vital role in hyperalgesia [22, 40, 41]. On the other hand, the pharmacological blockade of sympathetic activity has been shown to efficiently eliminate nociceptive sensation in clinical and preclinical studies [23–25, 42]. Moreover, previous studies have revealed that sympathetic hyperactivity and hyperinnervation are common in the myocardium after MI [18, 43], raising doubt whether sympathetic sprouting and sensory functional coupling are also present in the referred skin areas after MI. In this experiment, the left C8–T6 DRGs and skin of the left arm (0.3 × 0.3 cm^2) were removed for immunocytochemistry and western blotting at 3 and 7 days after MI operation. CGRP was used to label the nociceptive unmyelinated neurons or fibers, while TH was used to label the peripheral sympathetic post-ganglionic fibers [23]. The results indicated that the TH–IR fibers and CGRP-IR neurons/fibers increased in both the C8–T6 DRGs and forearm skin of rats at 3 and 7 days after MI (Figs 2 and 3), suggesting the sprouting of sympathetic fiber-endings in both DRGs and referred skin. Besides, the sprouted TH–IR sympathetic fibers surrounded the CGRP-IR DRG neurons to form a sympathetic-sensory coupling structure (Figs 2 and S3). The size of the DRG neurons involved in the sympathetic-sensory coupling structure was measured, and the diameters were mainly medium to small rather than large (Fig. S4). Furthermore, CGRP–IR and TH–IR proteins in the DRGs and referred skin were quantified using western blotting. Consistent with the data in the immunofluorescence study, the expression of TH and CGRP-positive proteins in model animals at 3 and 7 days after MI were markedly higher than those in controls (Figs 2C, E and 3C). These morphological results suggested that MI induces

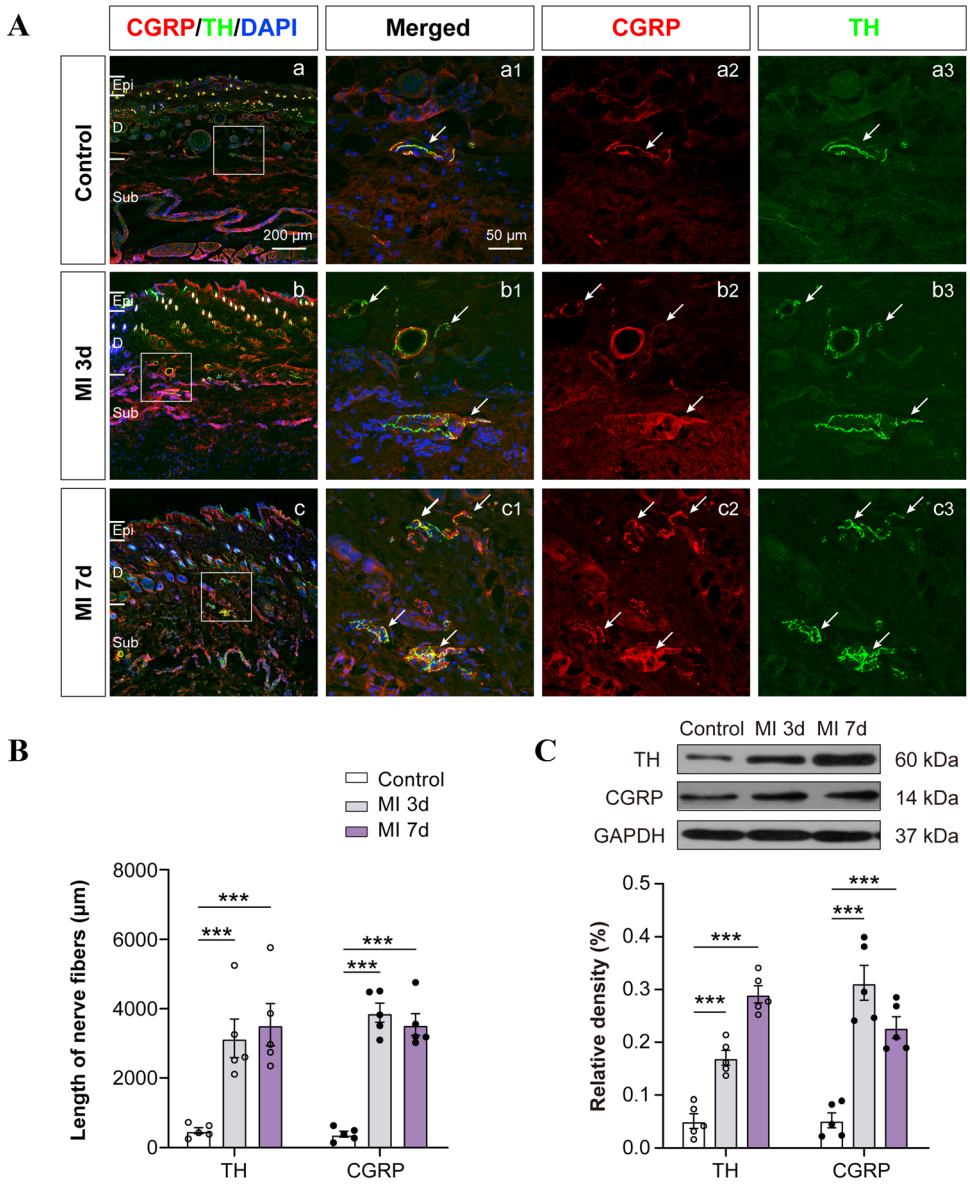

Fig. 3 Sprouting of sympathetic post-ganglionic fibers in the skin area where referred hypersensitivity is detectable after MI. **A** Representative images of immunoreactivity to calcitonin gene-related peptide (CGRP, red) and tyrosine hydroxylase (TH, green) in the forearm skin of control and MI rats at 3 and 7 days after LAD ligation. **a**1–3: higher power views of the boxed area in **a** (the same for **b** and **c**). White arrows indicate sprouted sympathetic terminals. Scale bar, 200 μm in **Aa**–**c**, and 50 μm in **Aa**1–**a**3, **Ab**1–**b**3, and **Ac**1–**c**3. **B** Lengths of CGRP+ and TH+ fibers in the forearm skin (n = 5/group, ***P <0.001). **C** Western blots showing increased levels of CGRP and TH protein expression in the sensitized skin of rats at days 3 and 7 post-MI (n = 5/group, ***P <0.001). One-way ANOVA with least significant difference multiple comparisons in **B**, **C**.

sympathetic hyperinnervation and sensory functional coupling in both the DRGs and referred skin areas at the same or adjacent spinal segments, and this might contribute to cardiac-referred hyperalgesia.

Sensitized Inputs from the Referred Area Augment Cardiac Sympathetic Nerve Hyperactivity in MI Rats

To explore the role of sympathetic sprouting and sensory coupling in DRGs and referred skin in MI, we monitored the SNA and VNA, as well as HR. To differentiate between afferents and efferents in the vagal trunk, we ligated the distal portion and hooked the proximal end of the nerve to record the output activity (Fig. S5). We first verified that MI for 7 days drove hyperactivity of the cardiac sympathetic nerve, but not the vagal nerve (Fig. 4B, C). MI also led to tachycardia in comparison with the control (Fig. 4D). These changes implied a functional compensation for impaired myocardium due to coronary ischemia to sustain heart pumping and circulation volume [15]. To estimate the role of somatic inputs from the referred area with sympathetic sprouting and sensory coupling, the left brachial plexus was clipped to destroy sensory inputs from the left forelimb, which lead to a decrease in the SNA and HR, but not the VNA, compared to pre-deafferentation (Fig. 4B, C). Moreover, tachycardia was recorded after deafferentation of the left brachial plexus, compared to the control. These results indicated that inputs from the referred area on the left arm are involved in sympathetic

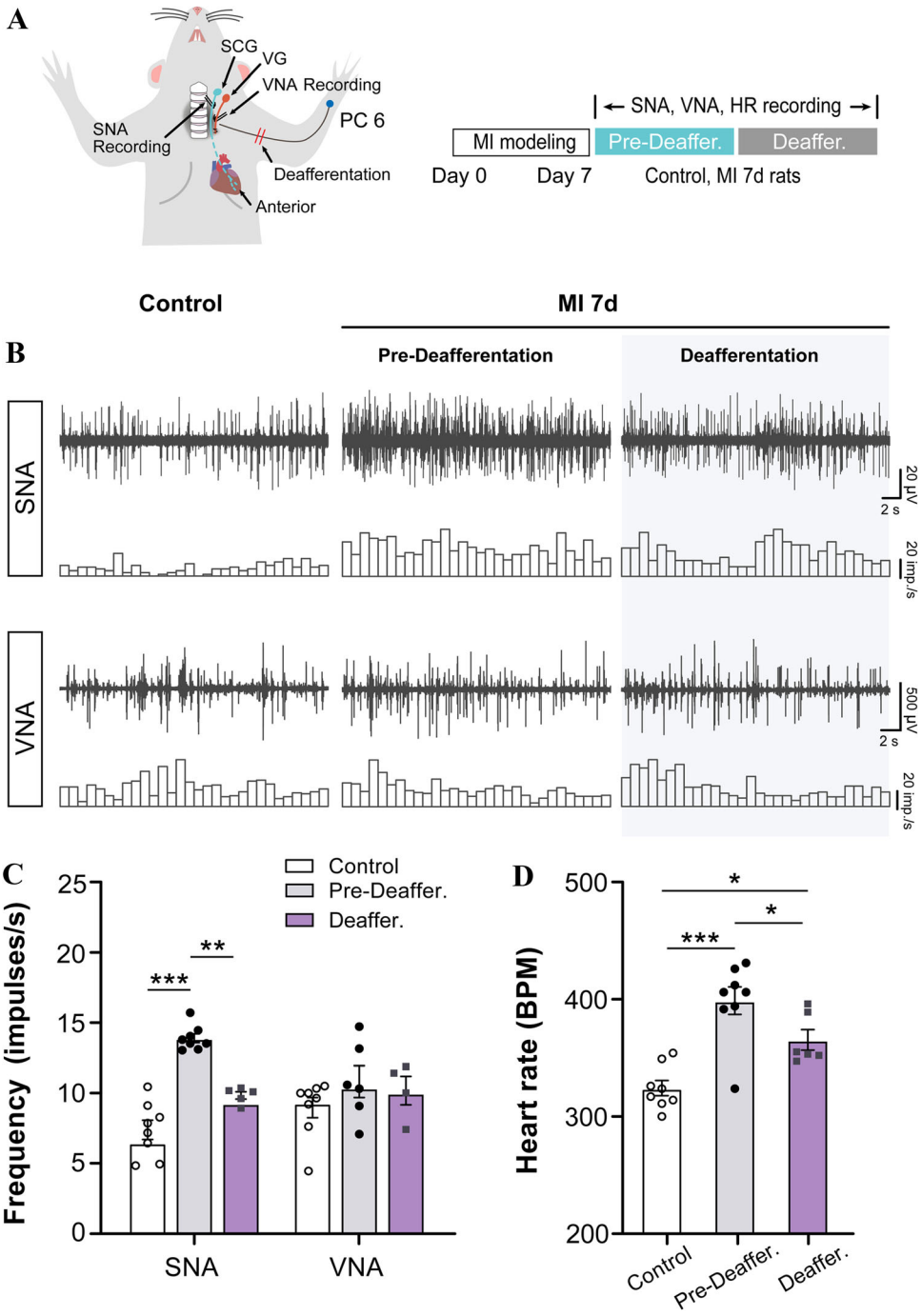

Fig. 4 MI rats show increased cardiac sympathetic activity that is attenuated by deafferentation of forelimb skin where referred mechanical sensitivity develops after MI. **A** Schematic of electrophysiological recording of post-ganglionic sympathetic nerve activity (SNA), vagal nerve activity (VNA), and heart rate (HR) in rats. Deafferentation of forearm is induced by clipping the brachial plexus. **B** Representative traces of SNA recorded from the superior cervical nerve (SCG) and VNA in the cervical vagus in control rats, and in MI rats before and after brachial plexus deafferentation. **C** Frequency of SNA and VNA in each group. **D** Quantification of HR. Deafferentation of the brachial plexus in MI rats attenuated the increased frequency of SNA and HR. (n = 8/group, $^{*}P$ <0.05, $^{**}P$ <0.01, $^{***}P$ <0.001). One-way ANOVA with the least significant difference multiple comparison tests.

nerve hyperactivity and cardiac acceleration in MI, and might act as functional compensation for the impaired myocardium.

In recent studies, somatic stimuli such as peripheral nerve stimulation and acupuncture have been shown to have a cardioprotective effect on cardiac dysfunction through the regulation of SNA or VNA [44, 45]. Here, we further explored the potential role of sensitized afferent inputs in the regulation of cardiac function under MI. We intensified the sensory inputs from the referred hypersensitivity areas by mechanical or thermal stimulation on the forearm (PC6) as a sensitized area, and this was then compared with the pre-stimulation baseline and with the same stimuli on non-sensitized areas in the hindlimb (SP 6). The results revealed that an innocuous brush, either on the forelimb or hindlimb, did not significantly influence the

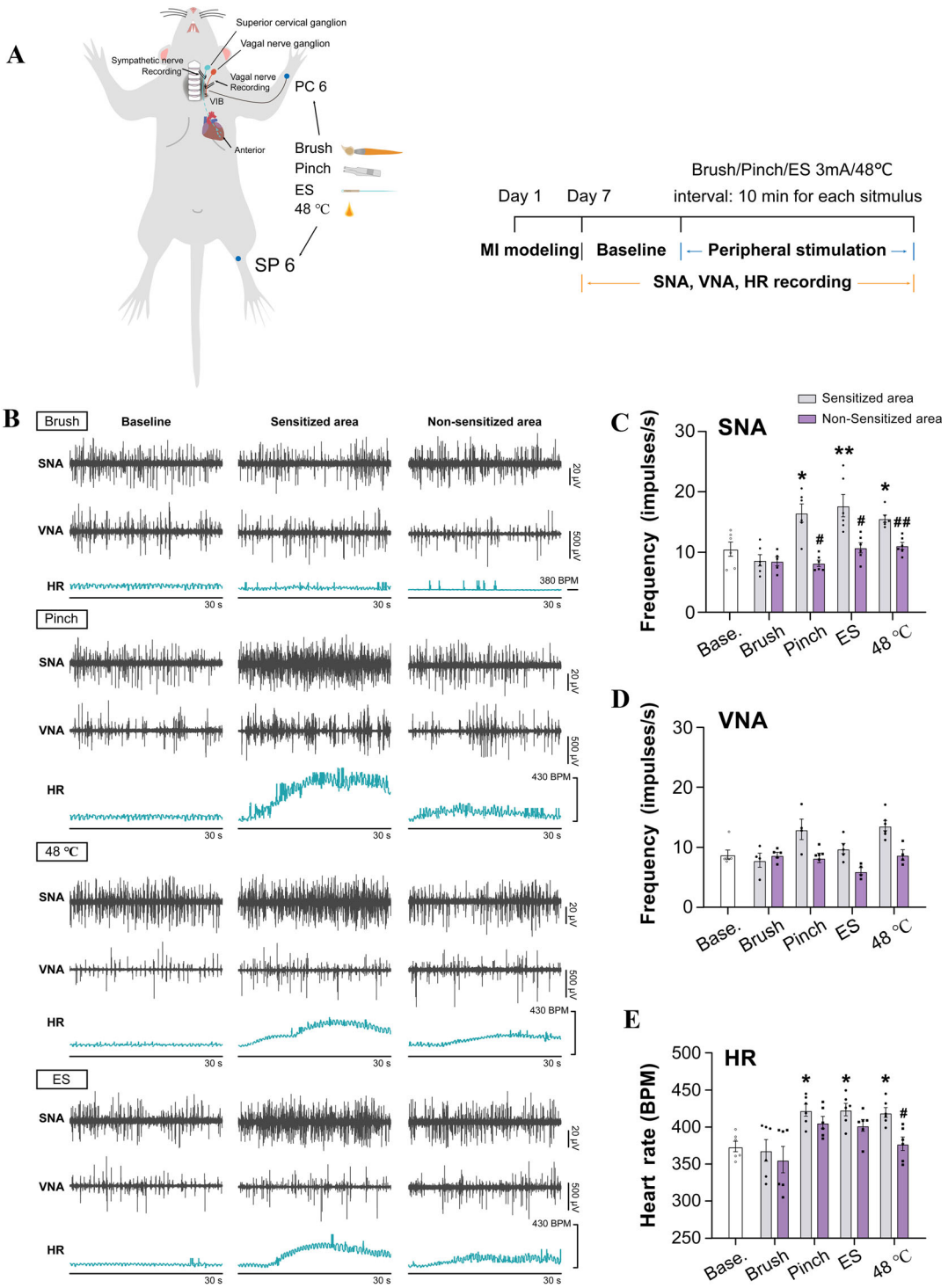

Fig. 5 Noxious stimulation applied to the somatic area where referred mechanical sensitivity develops after MI increases SNA and HR. **A** Schematic (left) and experimental protocol (right) of electrophysiological recording of SNA and VNA in MI rats. Peripheral non-noxious (brush) or noxious stimuli [pinch, 3-mA electrical stimulation (ES), noxious heat (48°C)] applied either to the sensitized (PC6 in the forearm) or unsensitized (SP6 in the hindlimb) areas in MI rats. **B** Representative traces of SNA, VNA, and HR in MI rats before (baseline) and after stimulation applied to the sensitized and unsensitized areas. **C–E** Frequencies of SNA (**C**), VNA (**D**) ,and HR (**E**) before and after stimulation (n = 4–6/group; $^{*}P$ <0.05, $^{**}P$ <0.01 *vs* baseline; $^{\#}P$ <0.05, $^{\#\#}P$ <0.01 *vs* sensitized area). Two-way ANOVA with Bonferroni test was used to compare groups, and the paired t-test was used to compare sensitized and non-sensitized areas in **C–E**.

SNA, VNA, and HR (Fig. 5), whereas a noxious pinch, ES at 3 mA, or thermal stimulation of 48°C at the left PC6 produced a significant increase in the SNA and HR compared to the baseline level. Moreover, more SNA was evoked by stimuli on the sensitized area of the forelimb than that on the non-sensitized area of the hindlimb. Regarding HR, only thermal stimulation of 48°C at the forelimb elicited more beats than that at the hindlimb. These findings collectively suggested that sensory inputs from the cardiac referred area result in sympathetic hyperexcitation and cardiac hyperactivity. Noxious stimuli on the referred area further evoked the augmentation of sympathetic and cardiac hyperactivity, which was stronger than that on the non-referred area.

Sympathetic-sensory Coupling in DRGs and Referred Skin Mediated by α_2AR Activation Is Involved in Cardiac Regulation After MI

Since α_2ARs activated by NE from the sprouted sympathetic terminals mediates the mechanism of hyperalgesia under neuropathic and inflammatory pain [23, 24], we explored the role of α_2ARs in the process of cardiac referred pain and cardiac regulation. We first found increased expression of α_2AR-IR fibers and sensory neurons in referred skin and C8–T6 DRGs at 7 days after MI surgery (Fig. 6). Then, we considered the pre-and post-synaptic strategy of α_2ARs in sympathetic-sensory coupling and its influence on cardiac function. DEX, a selective α_2AR agonist, induces presynaptic inhibition of the sympathetic fiber endings [23], whereas YOB, a selective α_2AR-antagonist, acts on post-synaptic sensory fiber endings. Both agents blocked the sympathetic-sensory interactions in the referred skin. It has been reported that NE released from sympathetic fiber-endings binds with both pre-and post-synaptic α_2ARs. Presynaptic α_2AR activation of the sympathetic nerve endings provides feedback inhibition on the release of NE, whereas post-synaptic α_2AR activation of the sensory nerve endings causes afferent sensitization [46, 47]. Here, we chose specific pharmacological strategies, in that DEX acted on the presynaptic α_2ARs to inhibit the release of NE [23], whereas YOB directly prevented the binding of NE with the post-synaptic α_2ARs [24, 47, 48]. In this study, these drugs were intradermally microinjected into the left forelimb (5 μg/20 μL) in different animals. Then, the EF, CO, and HR were measured by echocardiography to evaluate the cardiac function in both control and MI rats for 7 days, and noxious somatic stimulation at 3 mA ES was delivered to the forelimb.

The results indicated a decrease in EF and CO and an increase in HR of rats after MI for 7 days, compared to

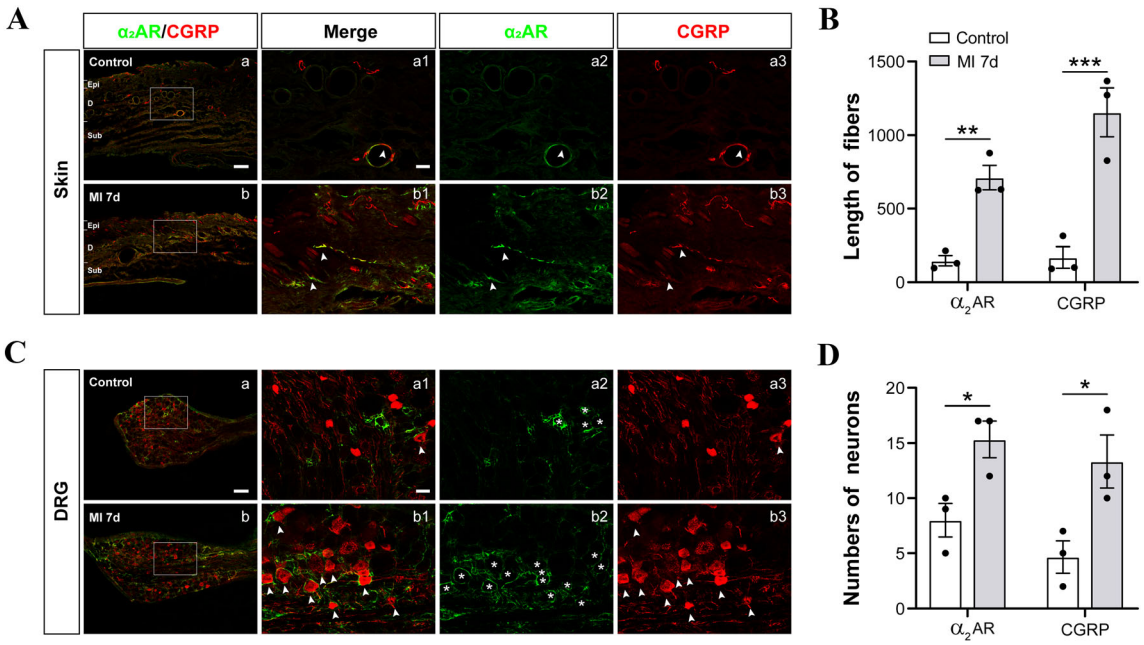

Fig. 6 MI induces increased numbers of α_2AR-positive fibers in the DRGs and skin. **A** Representative images of immunoreactivity to CGRP (red) and α_2AR (α_2 adrenoceptor, green) in the skin of control rats, and in the skin with referred mechanical hypersensitivity of MI rats. White arrowheads indicate CGRP+ fibers. Scale bar, 200 μm in **Aa**–**b**, and 50 μm in **Aa**1–**a**3, **Ab**1–**b**3. **B** Lengths of CGRP+ and α_2AR+ fibers in the skin (n = 3/group, $^{**}P$ <0.01, $^{***}P$ <0.001). **C** Representative images of CGRP and α_2AR immunoreactivity in the DRGs of control and MI rats. White arrowheads indicate CGRP+ fibers, and asterisks indicate α_2AR+ neurons. Scale bar, 200 μm in **Ca**–**b**, and 50 μm in **Ca**1–**a**3, **Cb**1–**b**3. **D** Numbers of CGRP+ and α_2AR+ neurons in DRGs (n = 3/group, $^{*}P$ <0.05). Independent t-test.

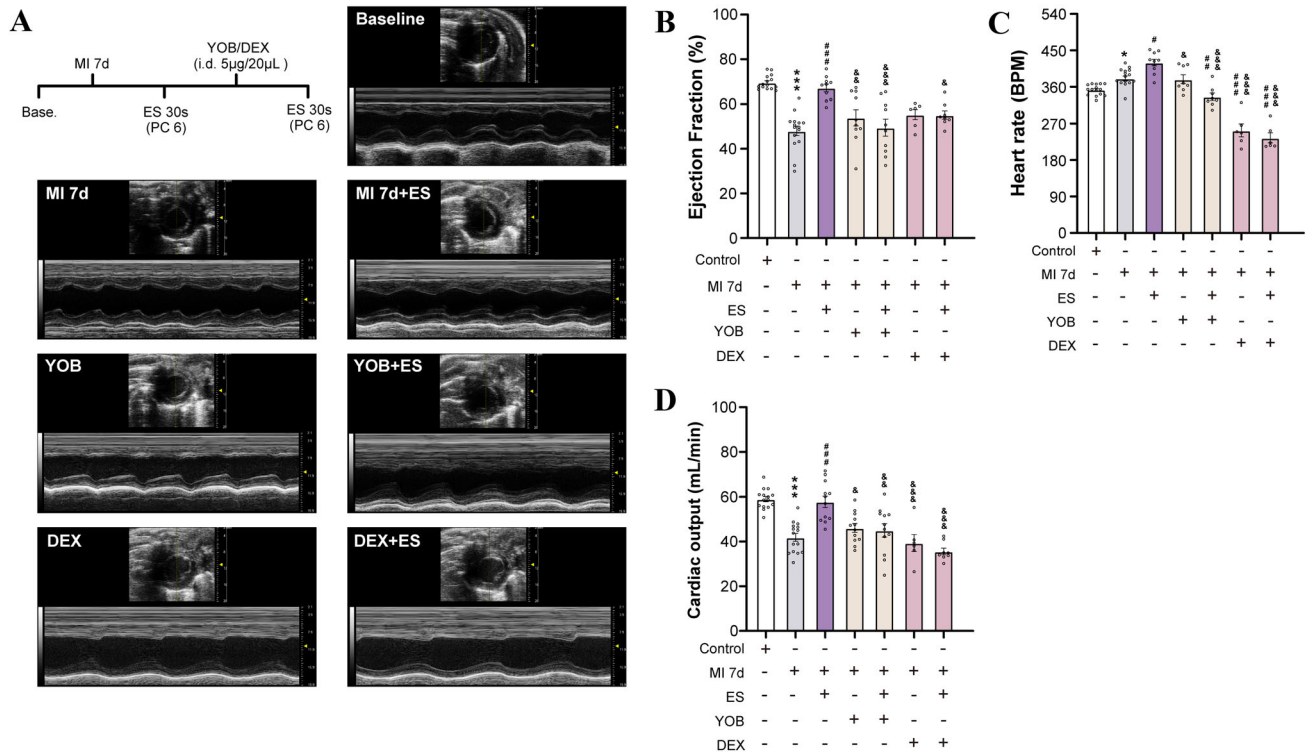

Fig. 7 Peripheral α_2ARs mediate the cardiac adjustment elicited by electrical stimulation in the skin area with referred mechanical hypersensitivity in MI rats. **A** Experimental protocol and representative echocardiography images of the left ventricle (LV) before and after drug treatment. **B–D** LV ejection fraction (**B**), heart rate (**C**), and cardiac output (**D**) in control rats, and in MI rats in response to electrical stimulation (ES, 3 mA, 15 Hz, 30 s), intradermal injection of yohimbine (YOB, 5 μg/20 μL, an α_2AR antagonist) and dexmedetomidine (DEX, 5 μg/20 μL, a potent and selective α_2AR agonist that inhibits norepinephrine release from synaptic vesicles) at the sensitized area (PC6) on the forelimb (n = 8–10/group; $^{*}P$ <0.05, $^{***}P$ <0.001, *vs* control; $^{\#}P$ <0.05, $^{\#\#\#}P$ <0.001, *vs* MI 7 days; $^{\&}P$ <0.05, $^{\&\&}P$ <0.01, $^{\&\&\&}P$ <0.001, *vs* MI 7 days+ES). One-way ANOVA with Bonferroni test in **B–D**.

those in the healthy control group (Fig. 7). On the other hand, noxious somatic stimulation of the left PC6 elevated the EF, CO, and HR to ameliorate cardiac function. YOB and DEX did not influence most cardiac functions, except that DEX caused a decrease in HR in MI rats. These results further demonstrated that YOB or DEX injection possibly attenuated the adjusting role of ES in cardiac function. Overall, our data confirmed that α_2ARs located at the peripheral sympathetic terminals and sensory axonal endings mediate the sympathetic-sensory interaction and the protective role of sensitized referred cutaneous inputs in cardiac functional regulation.

Discussion

The major findings of this study were the somatic hypersensitivity and sympathetic-sensory coupling in the DRGs and referred skin evoked by MI and the role of this coupling in the regulation of cardiac function. First, chronic MI not only led to hyperexcitation of the sympathetic nerve and tachycardia but also elicited postganglionic sympathetic fiber sprouting and hyperinnervation in the DRGs and referred skin, with mechanical hypersensitivity at spinal segments that were proximal to the heart. Sympathoexcitation induced by sensory inputs from referred somatic hyperalgesic areas was blocked by deafferentation of the brachial plexus and augmented by noxious stimuli on the referred area. Secondly, pharmacological blockade of α_2AR sympathetic-sensory coupling in the referred somatic areas attenuated the effects of ES on cardiac function. These findings collectively demonstrated that somatic referred pain triggered cardiac regulation *via* sympathetic-sensory interaction under chronic MI.

Sensory Inputs from Referred Hyperalgesia Are Involved in Sympathetic Hyperexcitation After MI

Although cardiac referred pain has been widely reported, the underlying implication remains elusive. Except for the convergence of viscerosomatic inputs at the spinal and supraspinal levels [1], early evidence using retrograde

fluorescent tracing in rats also showed that the bifurcation of the left C8–T1 DRG neurons innervate both the heart and left forelimb [49], suggesting a direct connection of sensory inputs between the heart and the referred left forelimb. Recent advances in the viscerosomatic convergence have demonstrated that the somatic and visceral C fibers monosynaptically converge onto one lamina I projection neuron in the spinal dorsal horn [50], which is strongly associated with referred pain. Clinical studies have reported that referred pain induced by angina pectoris is commonly displayed on the left shoulder and flexor portion of the left forelimb [51]. In this study, through Evans blue test and electrical Von Frey measurements, we also found that the cardiac referred area was distributed mainly on the left forelimb, chest, and upper back innervated by C6–T6 segments and within the cardiac innervation in rats (Fig. 1E–F) [9]. EB extravasation indicates that neurogenic inflammation and exudation of plasma protein occurs in the referred skin area of MI [52]. It has been reported that C-poly nociceptors, not Aδ, in the referred hyperalgesic area are driven to hyperexcitation and upregulation of hyperpolarization-activated current [53], which subsequently induces various bio-activators to cause neurogenic inflammation and hyperalgesia through the axon and dorsal root reflexes [29, 54]. Activation of C-poly nociceptors has also been identified as a key driver of induced somato-sympathetic or somato-visceral reflexes [55], which subsequently influence visceral function.

Pain has been suggested to not only represent unpleasant feelings but also to act as a homeostatic emotion and induce protective behavior for survival [10]. Here, we revealed that cardiac referred pain contributed to the regulation of cardiac function through involvement in MI-induced sympathetic hyperexcitation. Cell bodies of the cardiac sensory neurons reside in the T2–T6 DRGs [8], the peripheral terminals of which mainly innervate the anterior region of the left ventricle [9]. Specifically, the anterior myocardium is innervated by sympathetic fibers from the SCG [14], whereas the stellate ganglion predominantly innervates the dorsal side of the ventricular myocardium [14]. Recent studies have indicated that cardiac TRPV1 afferent signaling and purinergic receptors (P2) are excited under MI and subsequently play a vital role in sympathoexcitation-induced arrhythmogenic myocardium [19, 56]. Here, we found that ligation of the LAD led to overexcitation of the carotid branch from the SCG, the post-ganglionic cardiac sympathetic nerve.

The sympathetic nervous system is widely acknowledged to be crucial for survival, as it innervates all the vasculature that supplies oxygen and nutrients to the vital organs. Internal and external environmental changes result in the rapid activation of the sympathetic nervous system. Previous studies have reported that MI directly provoke cardiac SNA hyperactivation [13, 57, 58]. Given that the myocardial contractility of the left ventricle is impaired after ligating the LAD, sensory inputs from the ligated area subsequently drive the SNA overactivation [13, 57, 58], thus maintaining the stability of the volume and pressure of the circulating blood [15], as well as accelerating the metabolism of inflammatory agents around the impaired myocardium [59]. However, excessive and sustained sympathetic overdrive results in lethal arrhythmias or even cardiac death due to the deterioration of the oxygen supply and a direct or indirect increase in the oxygen demand [60, 61]. Recent studies have revealed that peripheral nociceptive sensory inputs have a cardioprotective effect on the MI model, suggesting that the activation of C-fibers leads the cardiac sympathetic nerve endings to release NE and bradykinin *via* the dorsal root reflex [11, 12]. Here, we document that the sensory inputs from the cardiac-referred hypersensitive area augmented cardiac sympathoexcitation and tachycardia instead of vagal activation through clipping the brachial plexus, which to some extent directly contributed to the cardiac homeostatic regulation in response to coronary ischemia induced by ligating the LAD. Moreover, SNA reacted differently to somatic stimulation in an intensity- and location-dependent manner. Consistent with previous studies [62, 63], noxious pinch, thermal, and ES stimuli, but not innocuous brushing, augmented the sympathoexcitation and resulted in tachycardia, the levels of which were higher than those evoked with the same stimulation of non-sensitized areas. That is because the visceral SNA excitation requires C-fiber activation following a noxious stimulus at the somatic area of proximal segment to the recorded viscera [62, 63]. We assumed that the role of sensory inputs and stimuli on the left forelimb in cardiac function was related to sympathetic-sensory coupling, the functional connection between body and heart. However, consecutive intervention or somatic therapy at areas of MI-induced referred hyperalgesia on sympathetic and cardiac functions needs to be explored further.

Some studies have demonstrated that peripheral nerve stimulation is cardioprotective and have suggested this as a potential therapeutic strategy for MI patients [64]. Recent studies have demonstrated that peripheral nerve stimulation at subcutaneous nerve or acupoints benefit the adjustment of sympathetic tone and ventricular arrhythmia under MI [44, 45, 65]. Low-intensity subcutaneous nerve electrical stimulation (ScNS) (0.25 mA) at the Xinshu acupoint (BL15, ∼5 cm lateral to the spine at the T5 level) or the left lateral thoracic nerve for two consecutive months exacerbates cardiac sprouting and has a pro-arrhythmic effect in ambulatory dogs; whereas high-intensity ScNS (3.5 mA) improves cardiac sympathoexcitation and has an anti-arrhythmic effect by remodeling the stellate ganglion

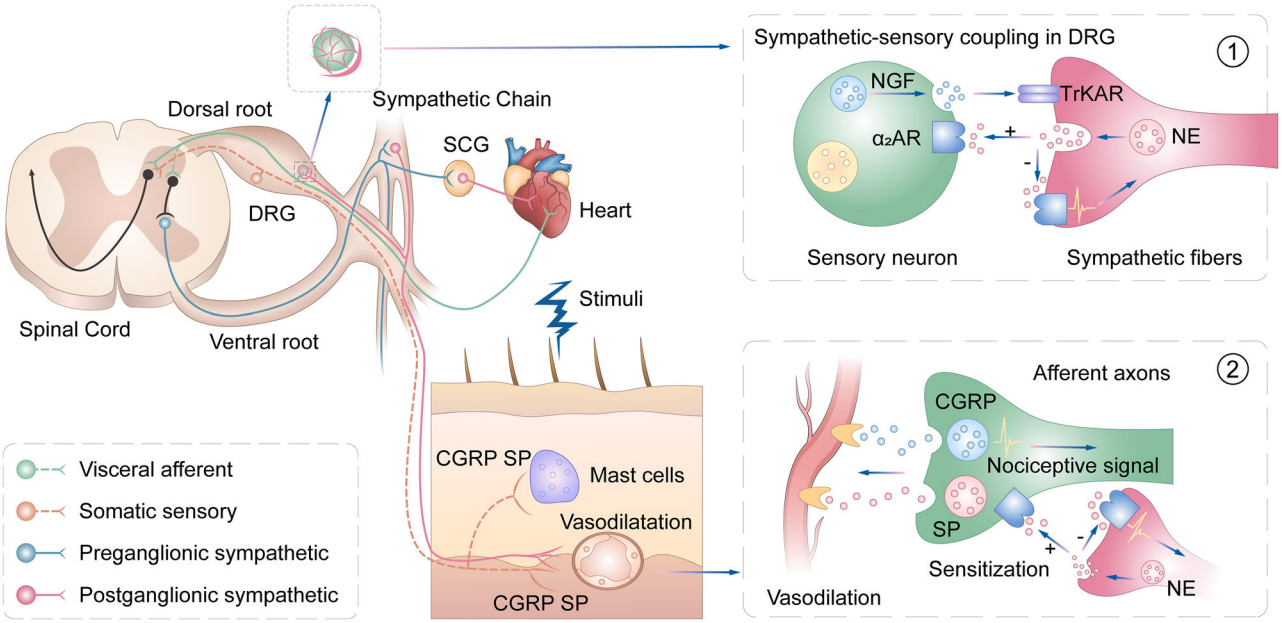

Fig. 8 Schematic of interactions between noxious sensory inputs from areas exhibiting referred pain and cardiac sympathetic outputs after MI. MI induces increased sympathetic activity and innervation in the myocardium, DRGs, and skin areas that develop referred pain. The sprouting of sympathetic fibers in DRGs is associated with an increased norepinephrine (NE), which sensitizes α_2AR-positive neurons and their peripheral nerve fibers. Noxious stimuli at the somatic area further augment sympathetic activity, which improves cardiac function. Blockade of α_2ARs at the sensory neurons and terminals or sympathetic fiber-endings inhibit sympathetic-sensory interaction. ① and ② illustrate sympathetic-sensory coupling in DRGs and in skin areas with referred pain. "+", excitatory action; "–", inhibitory action. NGF, nerve growth factors; TrkAR, TrkA receptor; α_2AR, alpha2 adrenoceptor; NE, norepinephrine; CGRP, calcitonin gene-related peptide; SP, substance P.

[65]. This means that the cardioprotective effect of peripheral nerve stimulation is correlated with the intensity of the stimulus. Notably, BL15 is located within the referred area of MI and was also indicated in the EB extravasation test in this study. Hence, the role of consecutive somatic stimulation at the referred area of MI in cardiac protection needs to be investigated further. Thus, we hypothesized that cardiac referred sensitization plays a vital role in the regulation of cardiac homeostasis by adjusting the sympathetic tone.

MI Leads to the Sprouting of Sympathetic Post-ganglionic Fibers and Sympathetic-sensory Coupling in Referred Skin and DRGs

Sympathetic sprouting has been reported for several years and has been found in skin and DRGs in various pain states [20, 22, 66–68]. However, the sprouting of sympathetic fibers into DRGs and referred skin following MI has rarely been investigated. DRGs, being a key component in the transmission of nociceptive sensory inputs and the signaling of proprioception to the central nervous system, play a vital role in pain and its management [69]. Previous studies have reported the sprouting of sympathetic terminals into DRGs [20, 70], skin [22], cornea [68], and periosteum [66] under neuropathic and inflammatory pain, with a tendency to sprout towards large and medium-sized sensory neurons (Aβ and Aδ) with ectopic discharging [71], and the formation of a basket-like structure that contributes to sensory sensitization [22, 40, 41]. Recent studies have reported that sympathetic post-ganglionic fibers also sprout into the heart and sympathetic ganglia such as the stellate and superior cervical ganglia under chronic MI [18, 72, 73], and this is responsible for lethal arrhythmias [72]. However, the role of MI in sympathetic sprouting in DRGs and the regulation of cardiac function should also be considered. Here, we found that MI not only led to sympathetic hyperactivity but also elicited post-ganglionic sprouting into DRGs and referred hypersensitive skin. Interestingly, sprouted fibers preferred surrounding medium to small DRG neurons rather than large to medium neurons in neuropathic and inflammatory pain, as small and medium neurons are predominantly responsible for visceral noxious input [74]. Moreover, sprouted sympathetic fibers release ATP and NE extracellularly to activate the sensory neurons by binding with P2 and α_2ARs, respectively [75]. As a result, more nociceptive inputs are transmitted to the spinal and supraspinal levels, which finally exacerbates central sensitization [76]. In addition, studies have shown that gender differences play a vital role in pain and affect

sensory perception, but the role of such differences in sympathetic-sensory coupling remains unknown and needs to be explored.

Since α_2ARs predominantly mediate the synaptic connections in sympathetic-sensory coupling [75], here, we found that MI led to more α_2ARs co-expressed with CGRP-labeled sensory neurons in DRGs and fibers in referred hypersensitive skin. α_2ARs are not only expressed on presynaptic (e.g. sympathetic terminals) but also on postsynaptic membrane (e.g. sensory neurons and fiber endings), hence more studies are required to precisely distinguish α_2AR-positive sensory fibers from sympathetic nerve fibers. Furthermore, we applied pharmacological strategies to explore the role of α_2AR-mediated sympathetic-sensory coupling in ES intervention through intradermally injected α_2AR agonists and antagonists into the referred skin area of MI. Presynaptic α_2ARs are autoinhibitory receptors, that mediate the feedback inhibition of NE release and produce the effect of chemical sympathectomy [47] (Fig. 8). DEX, a highly selective α_2AR agonist [23], was thereby used to block the sympathetic-sensory coupling *via* binding to presynaptic α_2ARs and then inhibit NE release. The NE released by sprouted sympathetic terminals is able to bind postsynaptic α_2ARs on sensory neurons in DRGs or peripheral axons in the skin, resulting in sensory neuron excitation. Hence, the blockade of postsynaptic α_2ARs using YOB could impair the sympathetic-sensory coupling and decrease the sensitized somatic inputs. That is why YOB and DEX had a similarly attenuated effect on cardiac function in response to ES at PC6. We hypothesize that the sympathetic-sensory coupling following MI augments the sensory inputs from the referred hypersensitive skin, which may be a novel target for peripheral nerve stimulation. Generally, long-term peripheral stimuli such as acupuncture and electrical stimulation of the transcutaneous nerve have been applied to induce cardioprotective effects in MI models and patients [44, 77–79]. Hence, the role of α_2ARs in the hyperalgesic skin or DRGs in the cardioprotective effects of long-term peripheral nerve stimulation requires further research.

Study Limitations and Clinical Implications

Previous studies have investigated the neurophysiological and pharmacological mechanisms of cardiac referred pain following MI at the level of the spinal or supraspinal sensory pathway and vagal cardiac afferents [1], whereas our study introduced a novel implication in the understanding of cardiac referred pain and cardiac homeostatic regulation under MI. Sensitized inputs from the referred hyperalgesic area augmented sympathetic hyperactivity and then played a positive role in reversing the decrease of blood circulation volume due to coronary occlusion. Furthermore, MI provoked not only sympathetic postganglionic hyperinnervation in the myocardium but also induced sympathetic terminal sprouting into DRGs and referred hyperalgesic skin [18, 72], where they coupled and sensitized medium-to-small sensory DRG neurons and cutaneous peripheral fibers *via* α_2ARs, which also mediated the effect of peripheral stimulation (ES). However, we only found an immediate effect of ES on SNA and cardiac function, whereas recent studies have reported that peripheral stimulation for no less than four weeks has a protective effect on sympathetic activity and arrhythmia [44, 65]. Therefore, further studies are needed to explore whether long-term stimulation in the referred area has the same effect. Although some studies have indicated that TH can be used not only to label sympathetic fibers but also C-low-threshold mechanical nociceptors in DRGs [80], TH is a rate-limiting enzyme for catecholamine and dopamine β-hydroxylase and is usually applied as an indicator for sympathetic fibers in sympathetic-sensory coupling studies. Hence, more specific markers for sympathetic fibers need to be used in future studies. Besides, due to the expression of α_2ARs on sympathetic terminals, sensory neurons, and peripheral afferents, more studies are required to identify the specific pre-or post-synaptic target that mediates the effect of ES, as well as to explore other related bioactivators that are involved in sympathetic-sensory coupling and the cardioprotective effect of peripheral stimulation.

Conclusion

The present study confirms that sensory inputs from referred hyperalgesia areas under MI play a positive role in the regulation of cardiac function by augmenting sympathoexcitation and sprouting of sympathetic terminals coupled with sensitized sensory neurons, as well as contributing to the effect of peripheral stimulation by activating α_2ARs in the referred areas.

Acknowledgments We are grateful to Dr. Haifa Qiao of Shaanxi University of Chinese Medicine and Dr. Yun Guan of Johns Hopkins University School of Medicine for constructive comments on an earlier version of the manuscript. We thank Dr. Wanzhu Bai, Dongsheng Xu, and Yangshuai Su of the Institute of Acupuncture and Moxibustion of the China Academy of Chinese Medical Sciences for technical assistance. This work was supported by the National Key R&D Program of China (2018YFC1704600) and the National Natural Science Foundation of China (81674085, 81904309).

Conflict of interest The authors declare no conflicts of interest.

References

1. Foreman RD, Garrett KM, Blair RW. Mechanisms of cardiac pain. Compr Physiol 2015, 5: 929–960.
2. Crea F. Doctor, I feel microvascular chest pain. Eur Heart J 2020, 41: 3219–3221.
3. Hobbs SF, Chandler MJ, Bolser DC, Foreman RD. Segmental organization of visceral and somatic input onto C3–T6 spinothalamic tract cells of the monkey. J Neurophysiol 1992, 68: 1575–1588.
4. Blair RW, Weber RN, Foreman RD. Characteristics of primate spinothalamic tract neurons receiving viscerosomatic convergent inputs in T3–T5 segments. J Neurophysiol 1981, 46: 797–811.
5. Blair RW, Ammons WS, Foreman RD. Responses of thoracic spinothalamic and spinoreticular cells to coronary artery occlusion. J Neurophysiol 1984, 51: 636–648.
6. Foreman RD, Blair RW, Weber RN. Viscerosomatic convergence onto T2–T4 spinoreticular, spinoreticular-spinothalamic, and spinothalamic tract neurons in the cat. Exp Neurol 1984, 85: 597–619.
7. Ammons WS, Girardot MN, Foreman RD. T2–T5 spinothalamic neurons projecting to medial thalamus with viscerosomatic input. J Neurophysiol 1985, 54: 73–89.
8. Vance WH, Bowker RC. Spinal origins of cardiac afferents from the region of the left anterior descending artery. Brain Res 1983, 258: 96–100.
9. Quigg M, Elfvin LG, Aldskogius H. Distribution of cardiac sympathetic afferent fibers in the Guinea pig heart labeled by anterograde transport of wheat germ agglutinin-horseradish peroxidase. J Auton Nerv Syst 1988, 25: 107–118.
10. Craig AD. A new view of pain as a homeostatic emotion. Trends Neurosci 2003, 26: 303–307.
11. Jones WK, Fan GC, Liao SY, Zhang JM, Wang Y, Weintraub NL. Peripheral nociception associated with surgical incision elicits remote nonischemic cardioprotection *via* neurogenic activation of protein kinase C signaling. Circulation 2009, 120: S1–S9.
12. Basalay M, Barsukevich V, Mastitskaya S, Mrochek A, Pernow J, Sjöquist PO, *et al*. Remote ischaemic pre- and delayed postconditioning - similar degree of cardioprotection but distinct mechanisms. Exp Physiol 2012, 97: 908–917.
13. Zekios KC, Mouchtouri ET, Lekkas P, Nikas DN, Kolettis TM. Sympathetic activation and arrhythmogenesis after myocardial infarction: Where do we stand? J Cardiovasc Dev Dis 2021, 8: 57.
14. Manousiouthakis E, Mendez M, Garner MC, Exertier P, Makita T. Venous endothelin guides sympathetic innervation of the developing mouse heart. Nat Commun 2014, 5: 3918.
15. Florea VG, Cohn JN. The autonomic nervous system and heart failure. Circ Res 2014, 114: 1815–1826.
16. Shen MJ, Zipes DP. Role of the autonomic nervous system in modulating cardiac arrhythmias. Circ Res 2014, 114: 1004–1021.
17. Chen PS, Chen LS, Cao JM, Sharifi B, Karagueuzian HS, Fishbein MC. Sympathetic nerve sprouting, electrical remodeling and the mechanisms of sudden cardiac death. Cardiovasc Res 2001, 50: 409–416.
18. Yokoyama T, Lee JK, Miwa K, Opthof T, Tomoyama S, Nakanishi H, *et al*. Quantification of sympathetic hyperinnervation and denervation after myocardial infarction by three-dimensional assessment of the cardiac sympathetic network in cleared transparent murine hearts. PLoS One 2017, 12: e0182072.
19. Yoshie K, Rajendran PS, Massoud L, Mistry J, Swid MA, Wu XH, *et al*. Cardiac $TRPV_1$ afferent signaling promotes arrhythmogenic ventricular remodeling after myocardial infarction. JCI Insight 2020, 5: 124477.
20. McLachlan EM, Jänig W, Devor M, Michaelis M. Peripheral nerve injury triggers noradrenergic sprouting within dorsal root Ganglia. Nature 1993, 363: 543–546.
21. Chung K, Lee BH, Yoon YW, Chung JM. Sympathetic sprouting in the dorsal root ganglia of the injured peripheral nerve in a rat neuropathic pain model. J Comp Neurol 1996, 376: 241–252.
22. Nascimento FP, Magnussen C, Yousefpour N, Ribeiro-da-Silva A. Sympathetic fibre sprouting in the skin contributes to pain-related behaviour in spared nerve injury and cuff models of neuropathic pain. Mol Pain 2015, 11: 59.
23. Wu JR, Chen H, Yao YY, Zhang MM, Jiang K, Zhou B, *et al*. Local injection to sciatic nerve of dexmedetomidine reduces pain behaviors, SGCs activation, NGF expression and sympathetic sprouting in CCI rats. Brain Res Bull 2017, 132: 118–128.
24. Moon DE, Lee DH, Han HC, Xie JG, Coggeshall RE, Chung JM. Adrenergic sensitivity of the sensory receptors modulating mechanical allodynia in a rat neuropathic pain model. Pain 1999, 80: 589–595.
25. Ogon I, Takebayashi T, Miyakawa T, Iwase T, Tanimoto K, Terashima Y, *et al*. Suppression of sympathetic nerve sprouting by local administration of an α-antagonist around the dorsal root ganglion in a lumbar radiculopathy model. Spine (Phila Pa 1976) 2018, 43: E321–E326.
26. Ogon I, Takebayashi T, Iwase T, Emori M, Tanimoto K, Miyakawa T, *et al*. Sympathectomy and sympathetic blockade reduce pain behavior *via* alpha-2 adrenoceptor of the dorsal root ganglion neurons in a lumbar radiculopathy model. Spine (Phila Pa 1976) 2015, 40: E1269–E1275.
27. de Couto G, Liu WX, Tseliou E, Sun BM, Makkar N, Kanazawa H, *et al*. Macrophages mediate cardioprotective cellular postconditioning in acute myocardial infarction. J Clin Invest 2015, 125: 3147–3162.
28. Lim M, Wang WQ, Liang L, Han ZB, Li ZJ, Geng J, *et al*. Intravenous injection of allogeneic umbilical cord-derived multipotent mesenchymal stromal cells reduces the infarct area and ameliorates cardiac function in a porcine model of acute myocardial infarction. Stem Cell Res Ther 2018, 9: 129.
29. Fang YH, Han S, Li XX, Xie YK, Zhu B, Gao XY, *et al*. Cutaneous hypersensitivity as an indicator of visceral inflammation *via* C-nociceptor axon bifurcation. Neurosci Bull 2021, 37: 45–54.
30. Lee MT, Chen YH, Mackie K, Chiou LC. Median nerve stimulation as a nonpharmacological approach to bypass analgesic tolerance to morphine: A proof-of-concept study in mice. J Pain 2021, 22: 300–312.
31. Azhar A, El-Bassossy HM. Pentoxifylline alleviates cardiac ischemia and dysfunction following experimental angina in insulin resistance. PLoS One 2014, 9: e98281.
32. Hedger JH, Webber RH. Anatomical study of the cervical sympathetic trunk and ganglia in the albino rat (*Mus norvegicus* albinus). Acta Anat (Basel) 1976, 96: 206–217.
33. Li B, Hu YL, Li XZ, Jin GQ, Chen XQ, Chen GJ, *et al*. Sirt1 antisense long noncoding RNA promotes cardiomyocyte proliferation by enhancing the stability of Sirt1. J Am Heart Assoc 2018, 7: e009700.
34. Kaufman A, Sato A, Sato Y, Sugimoto H. Reflex changes in heart rate after mechanical and thermal stimulation of the skin at various segmental levels in cats. Neuroscience 1977, 2: 103–109.
35. Kimura A, Ohsawa H, Sato A, Sato Y. Somatocardiovascular reflexes in anesthetized rats with the central nervous system intact or acutely spinalized at the cervical level. Neurosci Res 1995, 22: 297–305.
36. Yin CS, Jeong HS, Park HJ, Baik Y, Yoon MH, Choi CB, *et al*. A proposed transpositional acupoint system in a mouse and rat model. Res Vet Sci 2008, 84: 159–165.

37. Bobkiewicz A, Cwykiel J, Siemionow M. Anatomic variations of brachial and lumbosacral plexus models in different rat strains. Microsurgery 2017, 37: 327–333.
38. Bharali LAM, Lisney SJW. The relationship between unmyelinated afferent type and neurogenic plasma extravasation in normal and reinnervated rat skin. Neuroscience 1992, 47: 703–712.
39. Kuo DC, Oravitz JJ, DeGroat WC. Tracing of afferent and efferent pathways in the left inferior cardiac nerve of the cat using retrograde and transganglionic transport of horseradish peroxidase. Brain Res 1984, 321: 111–118.
40. Xie WR, Strong JA, Zhang JM. Increased excitability and spontaneous activity of rat sensory neurons following *in vitro* stimulation of sympathetic fiber sprouts in the isolated dorsal root ganglion. Pain 2010, 151: 447–459.
41. Zhang JM, Li HQ, Munir MA. Decreasing sympathetic sprouting in pathologic sensory ganglia: A new mechanism for treating neuropathic pain using lidocaine. Pain 2004, 109: 143–149.
42. Wang YL, Su YS, He W, Jing XH. Electroacupuncture relieved visceral and referred hindpaw hypersensitivity in colitis rats by inhibiting tyrosine hydroxylase expression in the sixth lumbar dorsal root ganglia. Neuropeptides 2019, 77: 101957.
43. Cao JM, Chen LS, KenKnight BH, Ohara T, Lee MH, Tsai J, *et al*. Nerve sprouting and sudden cardiac death. Circ Res 2000, 86: 816–821.
44. Yuan Y, Jiang ZL, Zhao Y, Tsai WC, Patel J, Chen LS, *et al*. Long-term intermittent high-amplitude subcutaneous nerve stimulation reduces sympathetic tone in ambulatory dogs. Heart Rhythm 2018, 15: 451–459.
45. Yuan Y, Zhao Y, Wong J, Tsai WC, Jiang ZL, Kabir RA, *et al*. Subcutaneous nerve stimulation reduces sympathetic nerve activity in ambulatory dogs with myocardial infarction. Heart Rhythm 2020, 17: 1167–1175.
46. Gil DW, Wang J, Gu C, Donello JE, Cabrera S, Al-Chaer ED. Role of sympathetic nervous system in rat model of chronic visceral pain. Neurogastroenterol Motil 2016, 28: 423–431.
47. Hein L, Altman JD, Kobilka BK. Two functionally distinct α2-adrenergic receptors regulate sympathetic neurotransmission. Nature 1999, 402: 181–184.
48. Ogon I, Takebayashi T, Miyakawa T, Iwase T, Tanimoto K, Terashima Y, *et al*. Attenuation of pain behaviour by local administration of alpha-2 adrenoceptor antagonists to dorsal root Ganglia in a rat radiculopathy model. Eur J Pain 2016, 20: 790–799.
49. McNeill DL, Burden HW. Convergence of sensory processes from the heart and left ulnar nerve onto a single afferent perikaryon: A neuroanatomical study in the rat employing fluorescent tracers. Anat Rec 1986, 214: 441–444.
50. Luz LL, Fernandes EC, Sivado M, Kokai E, Szucs P, Safronov BV. Monosynaptic convergence of somatic and visceral C-fiber afferents on projection and local circuit neurons in *Lamina* I. Pain 2015, 156: 2042–2051.
51. Løvlien M, Schei B, Gjengedal E. Are there gender differences related to symptoms of acute myocardial infarction? A Norwegian perspective. Prog Cardiovasc Nurs 2006, 21: 14–19.
52. Ferrell WR, Russell NJ. Extravasation in the knee induced by antidromic stimulation of articular C fibre afferents of the anaesthetized cat. J Physiol 1986, 379: 407–416.
53. Zhang M, Guo HY, Ma YY, Xu FF, Bai FH, Liang SR, *et al*. Acupoint sensitization is associated with increased excitability and hyperpolarization-activated current (ih) in C- but not Aδ-type neurons. Neuroscience 2019, 404: 499–509.
54. Sorkin LS, Eddinger KA, Woller SA, Yaksh TL. Origins of antidromic activity in sensory afferent fibers and neurogenic inflammation. Semin Immunopathol 2018, 40: 237–247.
55. Uchida S, Kagitani F, Sato-Suzuki I. Somatoautonomic reflexes in acupuncture therapy: A review. Auton Neurosci 2017, 203: 1–8.
56. Fu LW, Longhurst JC. A new function for ATP: Activating cardiac sympathetic afferents during myocardial ischemia. Am J Physiol Heart Circ Physiol 2010, 299: H1762–H1771.
57. Schomig A, Haass M, Richardt G. Catecholamine release and arrhythmias in acute myocardial ischaemia. Eur Heart J 1991, 12: 38–47.
58. Kolettis TM, Kontonika M, Barka E, Daskalopoulos EP, Baltogiannis GG, Tourmousoglou C, *et al*. Central sympathetic activation and arrhythmogenesis during acute myocardial infarction: Modulating effects of endothelin-B receptors. Front Cardiovasc Med 2015, 2: 6.
59. Raja SN. Role of the sympathetic nervous system in acute pain and inflammation. Ann Med 1995, 27: 241–246.
60. Kingma JG, Simard D, Rouleau JR. Influence of cardiac nerve status on cardiovascular regulation and cardioprotection. World J Cardiol 2017, 9: 508.
61. Deng Y, Tan X, Li ML, Wang WZ, Wang YK. Angiotensin-converting enzyme 2 in the rostral ventrolateral medulla regulates cholinergic signaling and cardiovascular and sympathetic responses in hypertensive rats. Neurosci Bull 2019, 35: 67–78.
62. Sato A, Schmidt RF. Somatosympathetic reflexes: Afferent fibers, central pathways, discharge characteristics. Physiol Rev 1973, 53: 916–947.
63. Noguchi E, Ohsawa H, Kobayashi S, Shimura M, Uchida S, Sato Y. The effect of electro-acupuncture stimulation on the muscle blood flow of the hindlimb in anesthetized rats. J Auton Nerv Syst 1999, 75: 78–86.
64. Hausenloy DJ, Erik BH, Peter F, Gerd H, André NG, Andrew R, *et al*. Cardiac innervation in acute myocardial ischaemia/reperfusion injury and cardioprotection. Cardiovasc Res 2019, 115: 1167–1177.
65. Wan JY, Chen M, Yuan Y, Wang Z, Shen CY, Fishbein MC, *et al*. Antiarrhythmic and proarrhythmic effects of subcutaneous nerve stimulation in ambulatory dogs. Heart Rhythm 2019, 16: 1251–1260.
66. Jimenez-Andrade JM, Mantyh PW. Sensory and sympathetic nerve fibers undergo sprouting and neuroma formation in the painful arthritic joint of geriatric mice. Arthritis Res Ther 2012, 14: R101.
67. Grelik C, Bennett GJ, Ribeiro-da-Silva A. Autonomic fibre sprouting and changes in nociceptive sensory innervation in the rat lower lip skin following chronic constriction injury. Eur J Neurosci 2005, 21: 2475–2487.
68. Marfurt CF, Ellis LC, Jones MA. Sensory and sympathetic nerve sprouting in the rat cornea following neonatal administration of capsaicin. Somatosens Mot Res 1993, 10: 377–398.
69. Liem L, van Dongen E, Huygen FJ, Staats P, Kramer J. The dorsal root ganglion as a therapeutic target for chronic pain. Reg Anesth Pain Med 2016, 41: 511–519.
70. Chung K, Yoon YW, Chung JM. Sprouting sympathetic fibers form synaptic varicosities in the dorsal root ganglion of the rat with neuropathic injury. Brain Res 1997, 751: 275–280.
71. Xie WR, Strong JA, Mao JX, Zhang JM. Highly localized interactions between sensory neurons and sprouting sympathetic fibers observed in a transgenic tyrosine hydroxylase reporter mouse. Mol Pain 2011, 7: 1744–8069.
72. Yin J, Wang Y, Hu HS, Li XL, Xue M, Cheng WJ, *et al*. P2X7receptor inhibition attenuated sympathetic nerve sprouting after myocardial infarctionviathe NLRP3/IL-1β pathway. J Cell Mol Med 2017, 21: 2695–2710.
73. Kong FJ, Liu SM, Xu CS, Liu J, Li GD, Li GL, *et al*. Electrophysiological studies of upregulated P2X7 receptors in rat

superior cervical Ganglia after myocardial ischemic injury. Neurochem Int 2013, 63: 230–237.
74. Sikandar S, Dickenson AH. Visceral pain: The ins and outs, the ups and Downs. Curr Opin Support Palliat Care 2012, 6: 17–26.
75. Devor M, Janig W, Michaelis M. Modulation of activity in dorsal root ganglion neurons by sympathetic activation in nerve-injured rats. J Neurophysiol 1994, 71: 38–47.
76. Peirs C, Seal RP. Neural circuits for pain: Recent advances and current views. Science 2016, 354: 578–584.
77. Yuan Y, Liu X, Wan JY, Wong J, Bedwell AA, Persohn SA, *et al*. Subcutaneous nerve stimulation for rate control in ambulatory dogs with persistent atrial fibrillation. Heart Rhythm 2019, 16: 1383–1391.
78. Stavrakis S, Humphrey MB, Scherlag BJ, Hu YQ, Jackman WM, Nakagawa H, *et al*. Low-level transcutaneous electrical vagus nerve stimulation suppresses atrial fibrillation. J Am Coll Cardiol 2015, 65: 867–875.
79. Lomuscio A, Belletti S, Battezzati PM, Lombardi F. Efficacy of acupuncture in preventing atrial fibrillation recurrences after electrical cardioversion. J Cardiovasc Electrophysiol 2011, 22: 241–247.
80. Brumovsky PR. Dorsal root ganglion neurons and tyrosine hydroxylase—an intriguing association with implications for sensation and pain. Pain 2016, 157: 314–320.